



Bifunctional, Copper-Doped, Mesoporous Silica Nanosphere-Modified, Bioceramic Scaffolds for Bone Tumor Therapy

Hongshi Ma^{1†}, Zhenjiang Ma^{1†}, Qufei Chen¹, Wentao Li¹, Xiangfei Liu², Xiaojun Ma³, Yuanqing Mao¹, Han Yang¹, Hui Ma^{1*} and Jinwu Wang^{1*}

¹ Shanghai Key Laboratory of Orthopaedic Implants, Department of Orthopaedic Surgery, Shanghai Ninth People's Hospital, Shanghai Jiao Tong University School of Medicine, Shanghai, China, ² Department of Orthopaedic Surgery, Shanghai Zhongye Hospital, Shanghai, China, ³ Department of Orthopedics, Shanghai General Hospital, Shanghai Jiao Tong University School of Medicine, Shanghai, China

OPEN ACCESS

Edited by:

Xijian Liu,
Shanghai University of Engineering
Sciences, China

Reviewed by:

Xiaojun Zhou,
Donghua University, China
Luodan Yu,
Shanghai University, China

*Correspondence:

Jinwu Wang
wangjw@shsmu.edu.cn
Hui Ma
Orthopain@163.com

[†]These authors share first authorship

Specialty section:

This article was submitted to
Chemical Biology,
a section of the journal
Frontiers in Chemistry

Received: 25 September 2020

Accepted: 26 October 2020

Published: 09 December 2020

Citation:

Ma H, Ma Z, Chen Q, Li W, Liu X,
Ma X, Mao Y, Yang H, Ma H and
Wang J (2020) Bifunctional,
Copper-Doped, Mesoporous Silica
Nanosphere-Modified, Bioceramic
Scaffolds for Bone Tumor Therapy.
Front. Chem. 8:610232.
doi: 10.3389/fchem.2020.610232

In the traditional surgical intervention procedure, residual tumor cells may potentially cause tumor recurrence. In addition, large bone defects caused by surgery are difficult to self-repair. Thus, it is necessary to design a bioactive scaffold that can not only kill residual tumor cells but also promote bone defect regeneration simultaneously. Here, we successfully developed Cu-containing mesoporous silica nanosphere-modified β -tricalcium phosphate (Cu-MSN-TCP) scaffolds, with uniform and dense nanolayers with spherical morphology via 3D printing and spin coating. The scaffolds exhibited coating time- and laser power density-dependent photothermal performance, which favored the effective killing of tumor cells under near-infrared laser irradiation. Furthermore, the prepared scaffolds favored the proliferation and attachment of rabbit bone marrow-derived mesenchymal stem cells and stimulated the gene expression of osteogenic markers. Overall, Cu-MSN-TCP scaffolds can be considered for complete eradication of residual bone tumor cells and simultaneous healing of large bone defects, which may provide a novel and effective strategy for bone tumor therapy. In the future, such Cu-MSN-TCP scaffolds may function as carriers of anti-cancer drugs or immune checkpoint inhibitors in chemo-/photothermal or immune-/photothermal therapy of bone tumors, favoring for effective treatment.

Keywords: Cu-containing mesoporous silica nanospheres, 3D printing, bifunctional scaffolds, photothermal tumor therapy, tissue regeneration

INTRODUCTION

The traditional therapy for bone tumors is surgical intervention to remove tumor lesions. However, surgical resection cannot ensure complete excision of all tumor cells, and residual tumor cells may cause tumor recurrence. In addition, large bone defects caused by surgery are difficult to self-repair. Therefore, it is crucial to develop a bioactive biomaterial, whose bifunctionality includes both killing residual tumor cells and promoting bone defect regeneration. Such a biomaterial would also demonstrate great potential for bone tumor therapy.

Mesoporous silica nanospheres (MSNs), one of the most popular drug/growth factor carriers, have been widely used in diagnostics and biomedicine (Tang et al., 2012; Mamaeva et al., 2013). However, considering the limited drug/growth factor loading percentage and targeting effect, the introduction of bioactive ions, such as Co and Cu ions, in MSN is expected to have sustained treatment effects (Yuan et al., 2012; Xia et al., 2014). Compared with growth factors or drugs, bioactive ions usually induce physiological effects at relatively low concentrations and are less sensitive to pH or temperature under microenvironmental conditions (Li H. et al., 2014). It is evident that bioactive ions (e.g., Co, Cu, and Si) could enhance the osteogenic ability of rabbit mesenchymal stem cells (rBMSCs) and inhibit active bone resorption to increase bone density (Mir et al., 2007). Therefore, it is promising to prepare bioactive ion-containing MSN with uniform morphology and satisfactory degradation performance for application in tissue engineering.

Given the importance and difficulty associated with regenerating large bone defects in tissue engineering, increasing efforts have been made to develop novel bioactive biomaterial-based scaffolds (Kaplan et al., 2020; Matai et al., 2020). The 3D printing method, as a rapid and individual process, has been widely used to fabricate bioactive scaffolds, which can provide a three-dimensional (3D) environment for cell growth and nutrition transfer (Kim et al., 2018; Hassan et al., 2019). Thus, to realize the aim of large bone defect regeneration, it is essential to design functional, bioactive ion-containing MSN-modified 3D-printing bioceramic scaffolds, with interconnected macropore structure, ordered mesostructure, and bioactive ions. To our knowledge, there are only a few bioactive ion-containing MSN-modified 3D-printing bioceramic scaffolds for tissue regeneration. However, reported ion-containing MSN-modified bioceramic scaffolds for bone tissue regeneration do not exhibit the ability of bone tumor therapy.

Recently, owing to its noninvasive and selective characteristics, photothermal therapy has received increasing attention (Chen et al., 2017; Liu et al., 2019; Zhang et al., 2019; Zhou et al., 2020). Compared with carbon-based agents and organic systems (polypyrrole, polyaniline, and polydopamine), Cu-based photothermal agents, such as CuS, Bi₂S₃, CuFeSe₂, and CuCo₂S₄, have excellent photothermal performance with the advantages of easy fabrication, tunable size, good photostability, and low cost (Liu and Su, 2014; Zhang et al., 2016; Figueroa et al., 2017; Li et al., 2017). Therefore, copper-based biomaterials have been hypothesized to have great potential for tumor treatment.

On the above basis, Cu-containing MSN-modified β -TCP scaffolds (Cu-MSN-TCP) were designed and prepared by 3D printing and spin coating method, with a hierarchically porous structure and functional surface. The excellent photothermal ability of bifunctional scaffolds were systematically investigated. Bifunctional scaffolds exhibited satisfactory photothermal tumor therapy efficiency *in vitro*. Moreover, the results indicated that bifunctional scaffolds had the effect of promoting the osteogenic capacities of rBMSCs. Therefore, the prepared Cu-containing MSN-modified β -TCP scaffolds have the possibility to treat large bone defects caused by tumor.

TABLE 1 | Primer sequences used in quantitative reverse-transcriptase polymerase chain reaction.

Gene	Primer sequences
Rabbit-VEGF-F	5'-CGCTGGATTCCATACTCAT-3'
Rabbit-VEGF-R	5'-TCTGCCCGTCTTCAGTG-3'
Rabbit-OPN-F	5'-TCTCAGAAGCAGAATCTCCTAAC-3'
Rabbit-OPN-R	5'-ATGGCTTTCATGGACTTACTC-3'
Rabbit-Runx2-F	5'-CCTTCCACTCTCAGTAAGAAGA-3'
Rabbit-Runx2-R	5'-TAAGTAAAGGTGGCTGGATAGT-3'
Rabbit-BSP-F	5'-GAGCCTATGAGGATGAGTACAGTTA-3'
Rabbit-BSP-R	5'-AAATGGTCGCCAAATGC-3'
Rabbit-BMP-2-F	5'-GGCCTTTGCTCGTAACCTT-3'
Rabbit-BMP-2-R	5'-TCCGCTGTTTGTGTTTCG-3'
Rabbit-GAPDH-F	5'-GACTTCAACAGTGCCACC-3'
Rabbit-GAPDH-R	5'-TGCTGTAGCCAATTCGT-3'

MATERIALS AND METHODS

Materials

β -TCP powder was purchased from Kunshan Chinese Technology New Materials Corporation (Kunshan, China). Cetyltrimethylammonium bromide (CTAB), ammonium fluoride (NH₄F), tetraethoxysilane (TEOS), copper nitrate trihydrate, pluronic F-127, calcein AM, ethidium homodimer-1, fluorescein isothiocyanate (FITC), and 4,6-diamidino-2-phenylindole (DAPI) were purchased from Sigma-Aldrich (Shanghai, China). Cell Counting Kit-8 (CCK-8) was purchased from Beyotime Biotechnology (China).

Synthesis of Cu-MSN-TCP Scaffolds

First, we used a 3D printing method to fabricate β -TCP scaffolds. Mixed inks (5 g of β -TCP powder and 3.4 g of F127 solution) were stirred to obtain a homogeneous mixture and were subsequently loaded in a printing tube and printed *via* a computer-assisted design model.

Second, 5% Cu containing-MSN (5% Cu-MSN) were synthesized according to a method reported previously (Shi et al., 2016). In brief, CTAB (1.8 g) and NH₄F (3 g) were dissolved in distilled water (500 ml) and stirred at 80°C for 1 h. Copper nitrate trihydrate [Cu(NO₃)₂•3H₂O: 0.51 g] was dissolved in ethanol solution (1 ml), which was mixed with TEOS (9 ml), and the mixture was added dropwise to the solution of CTAB (1.8 g) and NH₄F (3 g). Nanospheres were collected, washed three times, freeze-dried, and calcined for 6 h at 600°C.

Finally, to prepare Cu-MSN-TCP scaffolds, the Cu-MSNs were uniformly coated on β -TCP scaffolds *via* the spin coating method (Zhang et al., 2015). Cu-MSN (0.005 g) was dissolved in 1 ml of dichloromethane:ethanol (20:80 v/v) solution under ultrasonic treatment for 1 h. Then, β -TCP scaffolds were immersed in Cu-MSN solution for 30 s. Thereafter, 20 μ l Cu-MSN solution was coated on the surface of bioceramic scaffolds (β -TCP scaffolds) *via* spin coating at 500 rpm for 20 s. This procedure was repeated two, four, six, and eight times to

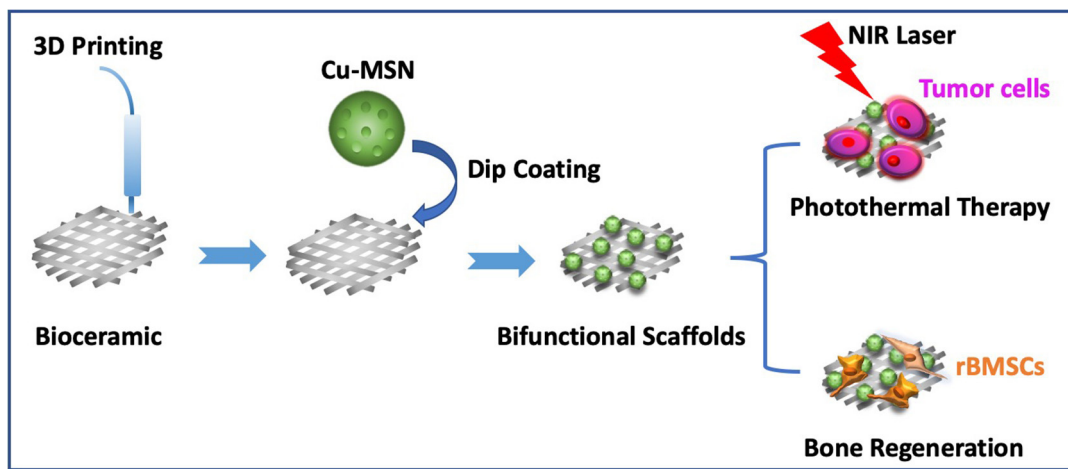


FIGURE 1 | Schematic illustration of prepared Cu-containing mesoporous silica nanospheres modified β -TCP scaffolds by combining 3D printing and spin coating method, and potential application of prepared scaffolds in photothermal tumor therapy and simultaneous osteogenesis promotion.

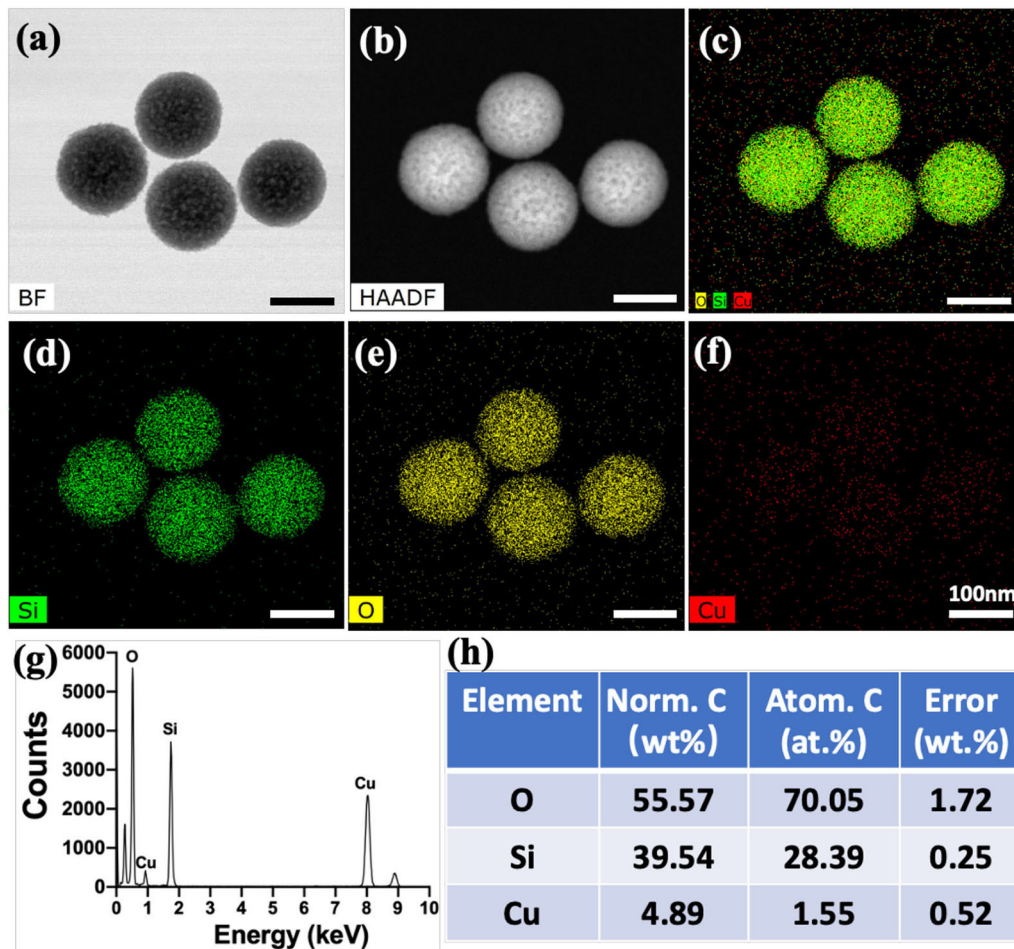
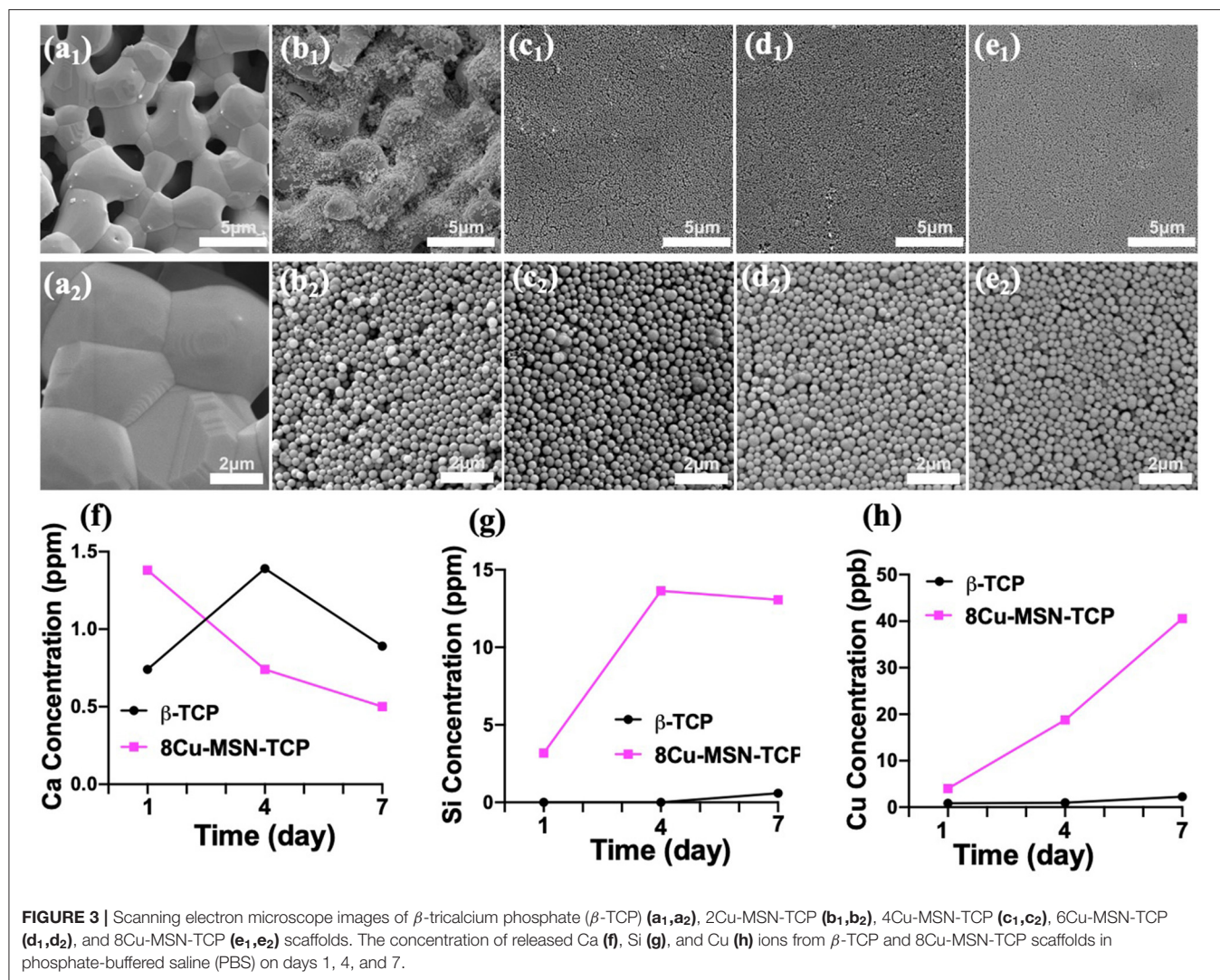


FIGURE 2 | Transmission electron microscope images of Cu-containing mesoporous silica nanospheres (Cu-MSN) in bright field (BF) model (a) and high-angle annular dark field (HAADF) model (b). Energy-dispersive spectrometry element mapping images of all (c), Si (d), O (e), and Cu (f) elements distributed in Cu-MSN. Energy-dispersive spectrometry analysis (g,h) of Cu-MSN.



prepare 2Cu-MSN-TCP, 4Cu-MSN-TCP, 6Cu-MSN-TCP, and 8Cu-MSN-TCP scaffolds, respectively.

Characterization

Microstructures of Cu-MSNs and Cu-MSN-TCP scaffolds were investigated using scanning electron microscopy (SEM, Mira3/MIRA3, TESCAN, Czech) and transmission electron microscopy (TEM, TALOS F200X, FEI, USA). Energy-dispersive spectroscopy (EDS) analysis was performed *via* TEM using an energy-dispersive spectrometer.

To detect the release of Cu, Si, and Ca ions from β -TCP and Cu-MSN-TCP scaffolds, the scaffolds were soaked in phosphate-buffered saline (PBS) for 1, 4, and 7 days (PBS volume to scaffold mass was 200 ml/g). On days 1, 4, and 7, the solution was collected and replaced with fresh PBS solution. The released Cu, Ca, and Si ion concentrations from the collected PBS solution were detected *via* inductively coupled plasma mass spectrometry (ICP-MS, I CAP Q, Thermo Fisher, Germany) and

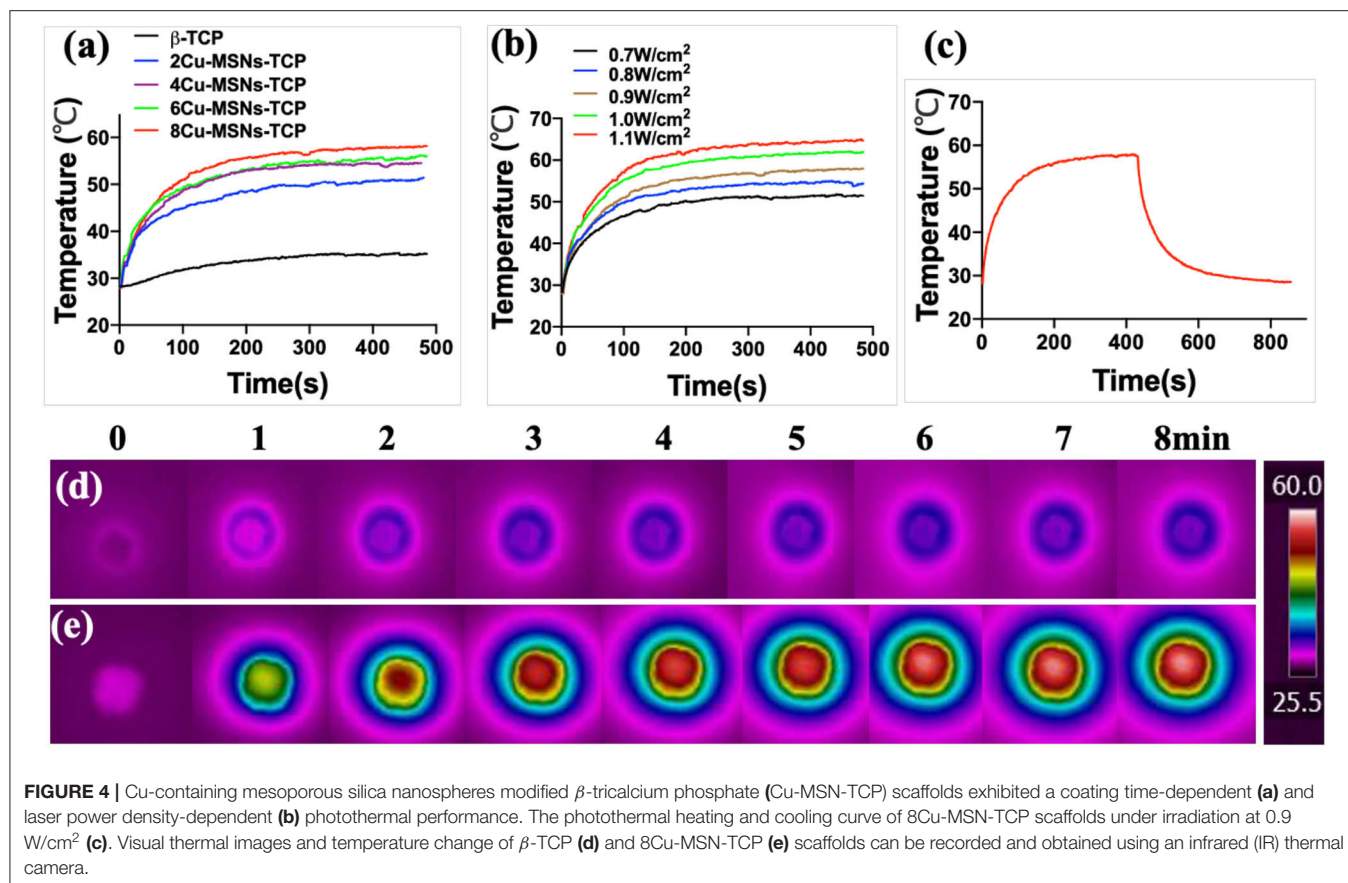
inductively coupled plasma optical spectrometry (iCAP 6300, Thermo, USA).

Photothermal Performance Test

To investigate their photothermal ability, 2Cu-MSN-TCP, 4Cu-MSN-TCP, 6Cu-MSN-TCP, and 8Cu-MSN-TCP scaffolds were irradiated for 500 s using a near-infrared (NIR) laser (power density: 0.9 W/cm²). In addition, the effect of different laser power densities on the final temperature of scaffolds was assessed, and the temperature was recorded using an IR thermal camera (Flir SC325, FLIR Systems Inc., USA).

In vitro Antitumor Efficacy

MG-63 cells (5.0×10^4), cultured in Dulbecco's modified Eagle's medium, were seeded in each well of a 48-well plate for 24 h (37°C, 5% CO₂) in an incubator and received the following four treatments: β -TCP scaffold without irradiation, β -TCP scaffold with radiation, 8Cu-MSN-TCP scaffold without irradiation, and 8Cu-MSN-TCP scaffold with irradiation. Three scaffolds in each



group were used for study. The scaffolds were gently placed into wells and irradiated using NIR laser (time: 15 min, power density: 2.5 W/cm²) to investigate the antitumor efficacy of bifunctional scaffolds against the surrounding tumor cells. Subsequently, the scaffolds were removed from the medium. Tumor cell viability was detected after 12 h using the CCK 8 assay according to the manufacturer's protocol. To obtain a more satisfactory antitumor efficacy, scaffolds were irradiated twice.

To visually observe the antitumor efficacy of bifunctional scaffolds following NIR light irradiation, calcein AM and ethidium homodimer-1 solutions were used for Live/Dead staining of tumor cells. Cells were observed using a confocal laser scanning microscope (CLSM; Leica TCS SP8, Wetzlar, Germany). Live tumor cells showed green fluorescence, whereas dead tumor cells showed red fluorescence.

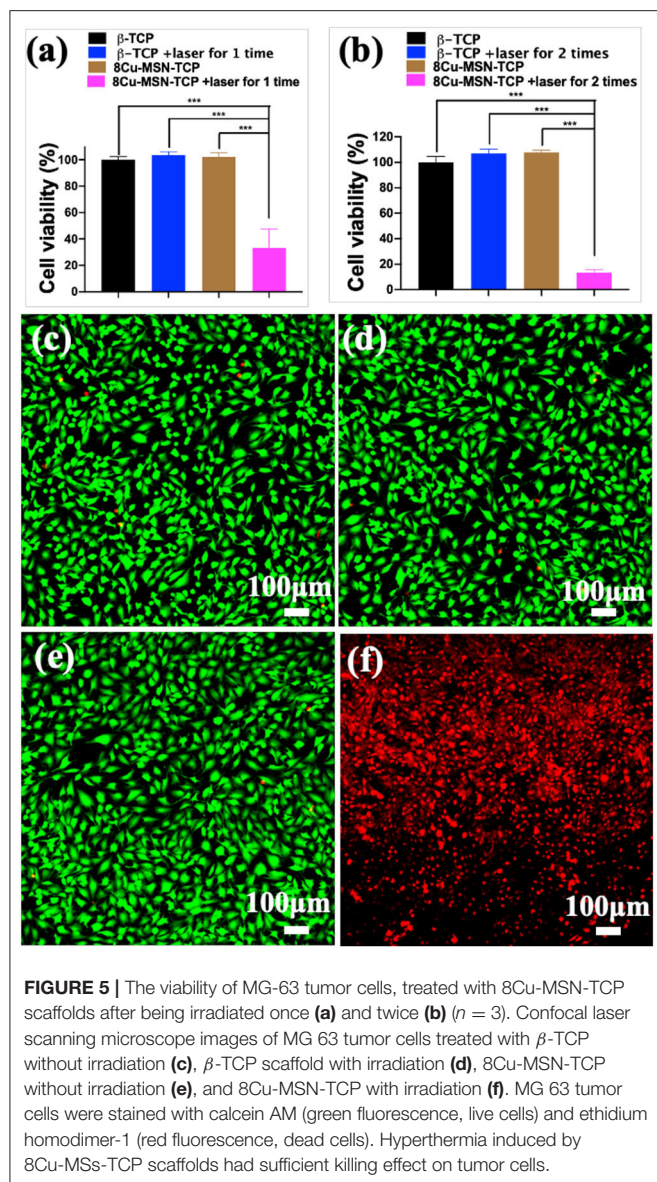
In vitro Biocompatibility and Osteogenic Differentiation Assay

The third passage of rabbit bone marrow-derived mesenchymal stem cells (rBMSCs, 3.0×10^4) was cultured on scaffolds (β -TCP and 8Cu-MSN-TCP) placed in 24-well plates containing the Minimum Essential medium for 1, 3, and 5 days. Three scaffolds in each group were used for study. On days 1, 3, and 5, cell viability was investigated by the CCK-8 assay and the absorbance measured using a microplate reader (Epoch, BIO-TEK, USA).

To observe cell attachment on scaffolds, 5.0×10^4 rBMSCs were cultured on scaffolds (β -TCP, 8Cu-MSN-TCP). Five days later, scaffolds were washed three times with PBS and subsequently treated with 2.5% glutaraldehyde for 20 min. Thereafter, samples were dehydrated using a gradient series of ethanol solutions (30, 50, 70, 80, 90, 95, and 100% v/v). Cell morphology on the scaffolds was observed *via* SEM.

Cell distribution and the cytoskeleton were characterized using a CLSM. After 5.0×10^4 rBMSCs were cultured on each scaffold (β -TCP, 8Cu-MSN-TCP) for 5 days, the scaffolds were treated with 2.5% glutaraldehyde. The cytoskeleton and nuclei of rBMSCs on scaffolds were stained with FITC solution for 1 h and DAPI solution for 10 min, respectively. Thereafter, the stained cells were observed by fluorescence microscopy (TCS SP8, Leica, Germany).

To investigate the effect of 8Cu-MSN-TCP scaffolds on the osteogenic differentiation of rBMSCs, 2.0×10^5 rBMSCs were cultured on each scaffold (β -TCP, 8Cu-MSN-TCP) in six-well plates for 7 days. Three scaffolds in each group were used for study. Real-time quantitative reverse transcription polymerase chain reaction (RT-qPCR) was conducted using SYBR Green qPCR Master Mix (TaKaRa, Japan) with a Light Cycler apparatus (CFX-Touch, Bio-Rad, USA) according to a previously reported method (Lin et al., 2019). The primers used in PCR are listed in **Table 1**.



RESULTS AND DISCUSSION

Fabrication and Characterization of Scaffolds

In this study, Cu-MSN-TCP scaffolds were fabricated *via* 3D printing and spin coating for the application of bone tumor therapy and tissue regeneration (Figure 1). First, 5% Cu-MSN were prepared using a soft-template method (CTAB). TEM and SEM results showed that all Cu-MSN exhibited a uniform spherical morphology with a well-ordered mesostructure, and the average diameter of Cu-MSN was approximately in a range of 120–145 nm (Figures 2a,b and Supplementary Figure 1). According to the element mapping images obtained from EDS, uniform distribution of Si, O, and Cu elements in Cu-MSN was observed (Figures 2c–f). EDS verified the existence of Cu, and the mass fraction of Cu accounted for 4.890.52% (Figures 2g,h). The

above results suggest successful synthesis of 5% Cu-MSN with an ideal structure, which is attributed to the cooperative assembly pattern between Cu and the structure-directing agent (CTAB), leading to a homogeneous distribution of Cu (Wei et al., 2009).

Thereafter, to prepare Cu-MSN-TCP scaffolds, the Cu-MSN solution was coated onto the surface of 3D-printed β -TCP scaffolds *via* the spin coating method. SEM analysis was conducted to assess the effect of spin coating times on the microstructure of Cu-MSN-TCP scaffolds. Low-magnification SEM images showed that after spin coating four, six, or eight times, Cu-MSN-TCP scaffolds were denser than those after two cycles (Figures 3a₁–e₁). As shown in Figures 3a₂–e₂, after spin coating four, six, or eight times, the nanolayers of Cu-MSN were uniformly deposited on the surface of β -TCP scaffolds. Herein, a combined method of 3D printing and spin coating was used to fabricate bioceramic scaffolds with hierarchical structures, including large pores and ordered mesostructures. Such an assembly strategy is extremely facile and effective.

Ion Release From Cu-MSN-TCP Scaffolds

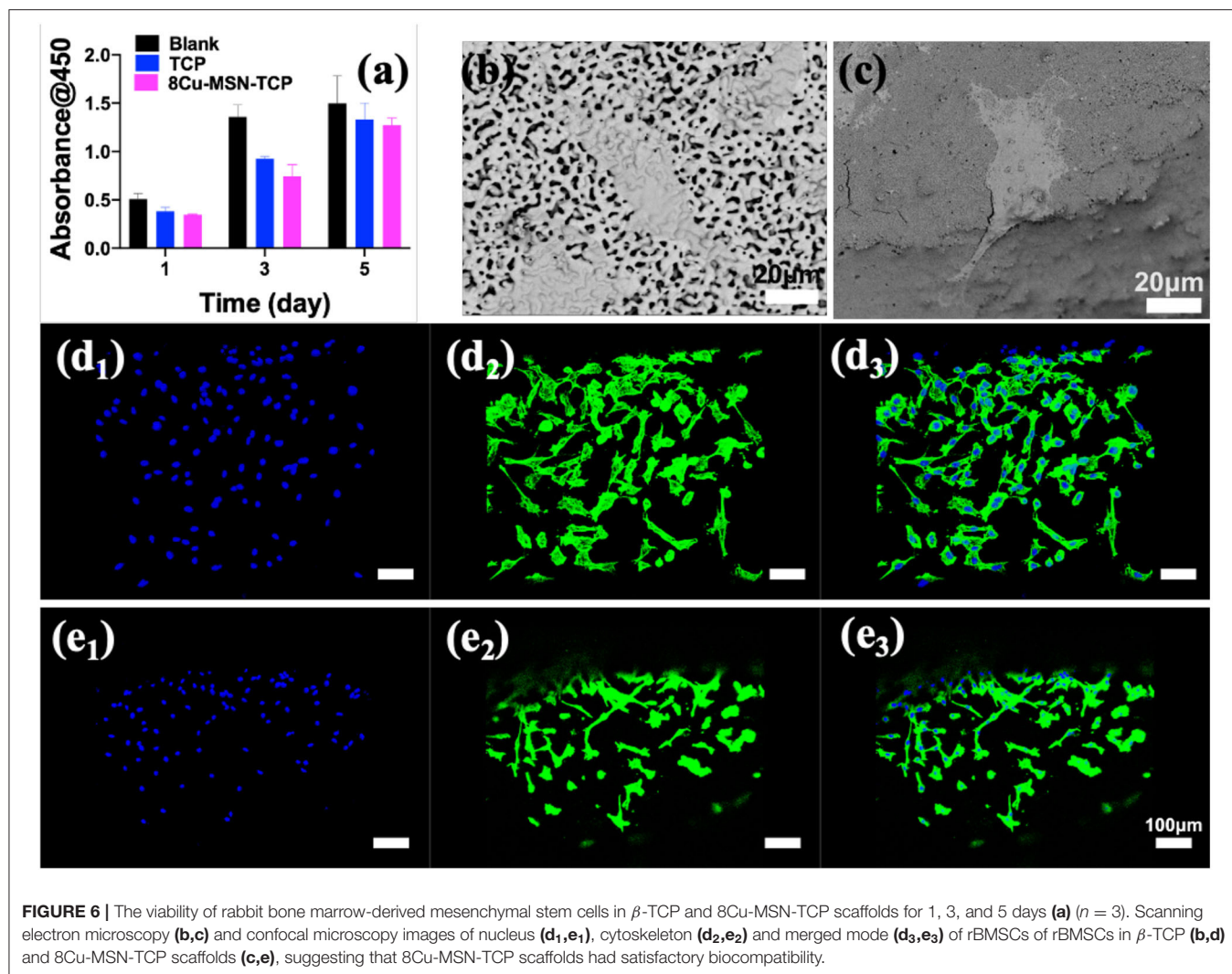
The release of Ca, Si, and Cu ions in PBS solution was detected *via* ICP-AES. As shown in Figures 3f–h, there was an evident continuous release of Si and Cu in 8Cu-MSN-TCP scaffolds. The concentration of Cu ions released from 8Cu-MSN-TCP scaffolds was approximately 4.01, 18.79, and 40.56 ppb on days 1, 4, and 7, respectively. The concentration of released Si ions from Cu-MSN-TCP scaffolds was 3.18, 13.64, and 13.07 ppm on days 1, 4, and 7, respectively. As a control, a negligible amount of released Cu and Si ions were detected from β -TCP scaffolds on days 1, 4, and 7. The continuous release of Si and Cu ions may favor osteogenesis during bone defect regeneration (Wu et al., 2019).

Photothermal Performance of Cu-MSN-TCP Scaffolds

Cu-MSN-TCP scaffolds exhibited coating time- and laser power density-dependent photothermal performance. The temperature of 8Cu-MSN-TCP scaffolds rapidly reached 58°C following NIR laser irradiation for 500 s (power density: 0.9 W/cm²), whereas the temperature of the β -TCP scaffold only increased by 7°C following NIR laser irradiation for 500 s at the same power density (0.9 W/cm²) (Figure 4a). In addition, the temperature of 8Cu-MSN-TCP scaffolds increased with an increase in NIR laser power density (Figure 4b). The temperature of 8Cu-MSN-TCP scaffolds exhibited a rapid increasing trend with NIR laser irradiation (Figure 4c). Visual thermal images and temperature change were recorded *via* an IR thermal camera, as shown in Figures 4d,e. The excellent photothermal ability of Cu-MSN-TCP scaffolds may be attributed to the d-d electronic transition of Cu ions, leading to the strong absorbance of the NIR light (Tian et al., 2011a,b; Li et al., 2017; Lu et al., 2018). These results indicated that Cu-MSN-TCP scaffolds can act as effective photothermal agents for killing tumor cells.

Photothermal Therapy Efficiency

To assess the efficiency of the photothermal therapy using 8Cu-MSN-TCP scaffolds, CCK 8 analysis was conducted. It was found that compared with the other three groups, the average viability



of MG-63 treated with the 8Cu-MSN-TCP scaffolds was 33.12% after being irradiated once (Figure 5a). This further decreased to 13.44% after second irradiation (Figure 5b), suggesting that hyperthermia induced by 8Cu-MSN-TCP scaffolds had a satisfactory killed tumor cells. CLSM images also showed that almost all tumor cells in the other three groups were viable (green fluorescence; Figures 5c–e). In contrast, a large amount of MG 63 tumor cells were dead (red fluorescence) in the 8Cu-MSN-TCP scaffolds + irradiation group (Figure 5f). Thus, Cu-MSN-TCP scaffolds are excellent photothermal agents, which exhibited effective photothermal therapy *in vitro* under NIR laser irradiation, as hyperthermia ($>50^{\circ}\text{C}$) can cause cell membrane damage, cause irreversible protein denaturation, and induce cell apoptosis and necrosis (Chu and Dupuy, 2014; Ma et al., 2016; Yin et al., 2016).

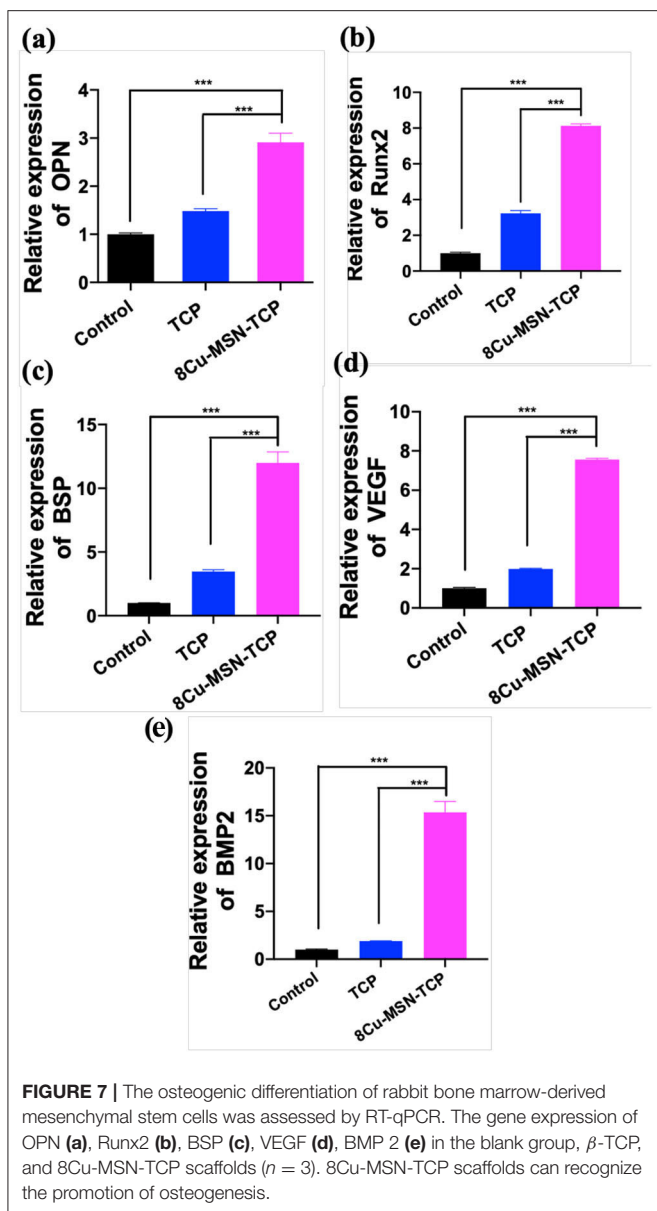
***In vitro* Biocompatibility of rBMSCs**

It is necessary to explore not only the photothermal therapeutic effect of bifunctional scaffolds but also their biological activity. The viability of rBMSCs in β -TCP and 8Cu-MSN-TCP scaffolds

at 1, 3, and 5 days is shown in Figure 6a. A cell proliferation increasing trend with culture time was evident in both β -TCP and 8Cu-MSN-TCP scaffold groups. Meanwhile, SEM (Figures 6b,c) and confocal microscopy (Figures 6d₁–d₃,e₁–e₃) were used to observe the morphology and attachment of rBMSCs on scaffolds on day 3. The 8Cu-MSN-TCP scaffolds supported cell adhesion and distribution, and rBMSCs were in close contact with the surface of Cu-MSN (Supplementary Figure 2). In addition, stained cells on 8Cu-MSN-TCP scaffolds exhibited a well-defined cytoskeleton as well as evident filopodia. Collectively, these results suggested that the Cu-MSN-TCP scaffolds had satisfactory biocompatibility.

***In vitro* Osteogenic Differentiation Assay**

RT-qPCR was used to evaluate the osteogenic ability of rBMSCs in β -TCP and 8Cu-MSN-TCP scaffolds. Gene expression of osteogenic markers, OPN, Runx2, BSP, BMP2, VEGF, on 8Cu-MSN-TCP scaffolds was significantly higher than that on blank and β -TCP scaffolds, suggesting that 8Cu-MSN-TCP scaffolds can promote osteogenesis (Figures 7a–e). It has been reported



that the constant release of Si and Ca ions from 8Cu-MSN-TCP scaffolds favors collagen synthesis, metabolism, and bone mineralization and increases the osteogenic differentiation of BMSCs and osteoblasts (Valerio et al., 2004; Wang et al., 2013; Li X. et al., 2014). Furthermore, Cu ions can modulate the immune environment, induce osteogenic factors, and suppress osteoclastogenic factors through immune cells (Mroczek-Sosnowska et al., 2015; Shi et al., 2016).

A key challenge in bone tissue engineering is the design and fabrication of bifunctional scaffolds for both therapy and regeneration. To our knowledge, there are only a few MSN-modified 3D-printing bioceramic scaffolds for bone tissue regeneration. However, reported ion-containing MSN-modified bioceramic scaffolds for bone tissue regeneration do not exhibit the ability of bone tumor therapy. One of important results was

that Cu-MSN-TCP scaffolds exhibited excellent photothermal performance, which can function as photothermal agents for killing tumor cells. Therefore, the novelty of this work is the fabrication of novel bifunctional scaffolds for both tumor therapy and tissue engineering.

There are several limitations to our study. First, because of excellent photothermal property of Cu-MSN-TCP scaffolds, they can kill tumor cells effectively under NIR laser irradiation. It would be worth investigating the effect of tumor therapy and bone regeneration of Cu-MSN-TCP scaffolds *in vivo*. In addition, considering the penetration depth of NIR laser, these bifunctional scaffolds also face some details and problems in clinical applications. Finally, Cu-MSN-TCP scaffolds can function as carriers of anti-cancer drugs or immune checkpoint inhibitors, and future work can focus on synergistic therapy of bone tumor.

CONCLUSION

A facile method of combining 3D printing and spin coating was applied to develop Cu-MSN-TCP scaffolds. Prepared 8Cu-MSN-TCP scaffolds had a dense uniform nanolayer of spherical morphology with a well-ordered mesostructure. Notably, these scaffolds exhibited excellent photothermal activity and could effectively kill tumor cells, owing to controlled hyperthermia induced under NIR laser irradiation. Furthermore, the scaffolds maintained satisfactory biocompatibility and evidently promoted gene expression of osteogenic markers OPN, Runx2, BSP, BMP 2, and VEGF. Therefore, this work indicates that the prepared Cu-MSN-TCP scaffolds can act as potential bifunctional biomaterials for photothermal bone cancer therapy and simultaneous bone defect regeneration. In the future, such Cu-MSN-TCP scaffolds may function as carriers of anti-cancer drugs or immune checkpoint inhibitors in chemo-/photothermal or immune-/photothermal therapy of bone tumors, favoring for effective treatment.

DATA AVAILABILITY STATEMENT

The datasets presented in this study can be found in online repositories. The names of the repository/repositories and accession number(s) can be found in the article/Supplementary Material.

AUTHOR CONTRIBUTIONS

JW and HuM contributed to study conception and design. HoM and ZM initiated and conducted this study. QC, WL, ZM, and HoM contributed to data collection, assembly, and analysis. HoM visualized data. XL, XM, and HY contributed to the literature review. HoM and ZM conceived this article and wrote the first draft. YM, HuM, and JW critically revised the article. All authors contributed to the article and approved the submitted version.

FUNDING

Funding for this work was provided by the National Key R&D Program of China (2018YFA0703000/2018YFB1105600), the National Natural Science Foundation of China (817723260), China Postdoctoral Science Foundation (Grant No. 2018M642042), the National Postdoctoral Program for Innovative Talents (Grant No. BX20180194), Project of Shanghai Science and Technology Commission (18441903700/19XD1434200/18431903700), Two-hundred Talent Support (20152224), Project of Shanghai Science and Technology Commission (17411960100), Project of Shanghai Jiading National Health and Family Planning Commission (KYXM 2018-KY-03), Project of Shanghai Bao Shan Science and Technology Commission (18-E-28), the National Natural Science Foundation of China (Grant No.

31900945), and research project of Jiading Agricultural and Social Undertaking (JDKY-2016-W04).

ACKNOWLEDGMENTS

The authors acknowledge funding from the National Key R&D Program of China (2018YFA0703000/2018YFB1105600), China Postdoctoral Science Foundation (Grant No. 2018M642042), and the National Postdoctoral Program for Innovative Talents (Grant No. BX20180194).

SUPPLEMENTARY MATERIAL

The Supplementary Material for this article can be found online at: <https://www.frontiersin.org/articles/10.3389/fchem.2020.610232/full#supplementary-material>

REFERENCES

- Chen, W., Ouyang, J., Liu, H., Chen, M., Zeng, K., Sheng, J. P., et al. (2017). Black phosphorus nanosheet-based drug delivery system for synergistic photodynamic/photothermal/chemotherapy of cancer. *Adv. Mat.* 29:1603864. doi: 10.1002/adma.201603864
- Chu, K. F., and Dupuy, D. E. (2014). Thermal ablation of tumours: biological mechanisms and advances in therapy. *Nat. Rev. Cancer* 14, 199–208. doi: 10.1038/nrc3672
- Figueroa, L. A., Alvarez, O. M., Cruz, J. S., Contreras, R. G., Hernández, F. J., and Arrocena, M. C. A. (2017). Nanomaterials made of non-toxic metallic sulfides: a systematic review of their potential biomedical applications. *Mater. Sci. Eng. C* 76, 1305–1315. doi: 10.1016/j.msec.2017.02.120
- Hassan, M. N., Yassin, M. A., Suliman, S., Lie, S. A., Gjengedal, H., and Mustafa, K. (2019). The bone regeneration capacity of 3D-printed templates in calvarial defect models: a systematic review and meta-analysis. *Acta Biomater.* 91, 1–23. doi: 10.1016/j.actbio.2019.04.017
- Kaplan, B., Merdler, U., Szklanny, A. A., Redenski, I., Guo, S., Bar-Mucha, Z., et al. (2020). Rapid prototyping fabrication of soft and oriented polyester scaffolds for axonal guidance. *Biomaterials* 251:120062. doi: 10.1016/j.biomaterials.2020.120062
- Kim, J. A., Yun, H. S., Choi, Y. A., Kim, J. E., Choi, S. Y., Kwon, T. G., et al. (2018). Magnesium phosphate ceramics incorporating a novel indene compound promote osteoblast differentiation *in vitro* and bone regeneration *in vivo*. *Biomaterials* 157, 51–61. doi: 10.1016/j.biomaterials.2017.11.032
- Li, B., Yuan, F. K., He, G. J., Han, X. Y., Wang, X., Qin, J. B., et al. (2017). Ultrasmall CuCo₂S₄ nanocrystals: all-in-one theragnosis nanoplatfrom with magnetic resonance/near-infrared imaging for efficiently photothermal therapy of tumors. *Adv. Funct. Mater.* 27:1606218. doi: 10.1002/adfm.201606218
- Li, H., Xue, K., Kong, N., Liu, K., and Chang, J. (2014). Silicate bioceramics enhanced vascularization and osteogenesis through stimulating interactions between endothelia cells and bone marrow stromal cells. *Biomaterials* 35, 3803–3818. doi: 10.1016/j.biomaterials.2014.01.039
- Li, X., He, Q., and Shi, J. (2014). Global gene expression analysis of cellular death mechanisms induced by mesoporous silica nanoparticle-based drug delivery system. *ACS Nano* 8, 1309–1320. doi: 10.1021/nn4046985
- Lin, R. C., Deng, C. J., Li, X. X., Liu, Y. Q., Zhang, M., Qin, C., et al. (2019). Copper-incorporated bioactive glass-ceramics inducing anti-inflammatory phenotype and regeneration of cartilage/bone interface. *Theranostics* 9, 6300–6313. doi: 10.7150/thno.36120
- Liu, S., and Su, X. G. (2014). The synthesis and application of I-III-VI type quantum dots. *RSC Adv.* 4, 43415–43428. doi: 10.1039/C4RA05677A
- Liu, T., Shen, S., Huang, Y., Zhang, X., Lai, Z., Tran, T. H., et al. (2019). Controllable growth of Au nanostructures onto MoS₂ nanosheets for dual-modal imaging and photothermal-radiation combined therapy. *Nanoscale* 11:22788. doi: 10.1039/C9NR06513J
- Lu, Y., Li, L. H., Lin, Z. F., Wang, L. P., Lin, L. J., Li, M., et al. (2018). A new treatment modality for rheumatoid arthritis: combined photothermal and photodynamic therapy using Cu₇2S₄ nanoparticles. *Adv. Healthc. Mater.* 7:1800013. doi: 10.1002/adhm.201800013
- Ma, H., Jiang, C., Zhai, D., Luo, Y., Chen, Y., Lv, F., et al. (2016). A bifunctional biomaterial with photothermal effect for tumor therapy and bone regeneration. *Adv. Funct. Mater.* 26, 1197–1208. doi: 10.1002/adfm.201504142
- Mamaeva, V., Sahlgren, C., and Linden, M. (2013). Mesoporous silica nanoparticles in medicine-recent advances. *Adv. Drug Deliv. Rev.* 65, 689–702. doi: 10.1016/j.addr.2012.07.018
- Matai, I., Kaur, G., Seyedsalehi, A., McClinton, A., and Laurencin, C. T. (2020). Progress in 3D bioprinting technology for tissue/organ regenerative engineering. *Biomaterials* 226:119536. doi: 10.1016/j.biomaterials.2019.119536
- Mir, E., Hossein-Nezhad, A., Bahrami, A., Bekheirnia, M. R., Javadi, E., and Naderi, A. A. (2007). Adequate serum copper concentration could improve bone density, postpone bone loss and protect osteoporosis in women. *Iran. J. Public Health* 36, 24–29. Available online at: <https://ijph.tums.ac.ir/index.php/ijph/article/view/1522>
- Mroczek-Sosnowska, N., Sawosz, E., Vadalasetty, K., Łukasiewicz, M., Niemiec, J., Wierzbicki, M., et al. (2015). Nanoparticles of copper stimulate angiogenesis at systemic and molecular level. *Inter. J. Mol. Sci.* 16, 4838–4849. doi: 10.3390/ijms16034838
- Shi, M. C., Chen, Z. T., Farnaghi, S., Friis, T., Mao, X. L., Xiao, Y., et al. (2016). Copper-doped mesoporous silica nanospheres, a promising immunomodulatory agent for inducing osteogenesis. *Acta Biomater.* 30, 334–344. doi: 10.1016/j.actbio.2015.11.033
- Tang, F. Q., Li, L. L., and Chen, D. (2012). Mesoporous silica nanoparticles: synthesis biocompatibility and drug delivery. *Adv. Mater.* 24, 1504–1534. doi: 10.1002/adma.201104763
- Tian, Q., Jiang, F., Zou, R., Liu, Q., Chen, Z., Zhu, M., et al. (2011a). Hydrophilic Cu₉S₅ nanocrystals: a photothermal agent with a 25.7% heat conversion efficiency for photothermal ablation of cancer cells *in vivo*. *ACS Nano* 5, 9761–9771. doi: 10.1021/nn203293t
- Tian, Q., Tang, M., Sun, Y., Zou, R., Chen, Z., Zhu, M., et al. (2011b). Hydrophilic flower-like CuS superstructures as an efficient 980 nm laser-driven photothermal agent for ablation of cancer cells. *Adv. Mater.* 23, 3542–3547. doi: 10.1002/adma.201101295
- Valerio, P., Pereira, M. M., Goes, A. M., and Leite, M. F. (2004). The effect of ionic products from bioactive glass dissolution on osteoblast proliferation and collagen production. *Biomaterials* 25, 2941–2948. doi: 10.1016/j.biomaterials.2003.09.086
- Wang, C., Lin, K., Chang, J., and Sun, J. (2013). Osteogenesis and angiogenesis induced by porous β-CaSiO₃/PDLGA composite scaffold via activation of AMPK/ERK1/2 and PI3K/Akt pathways. *Biomaterials* 34, 64–77. doi: 10.1016/j.biomaterials.2012.09.021

- Wei, K., Guo, W., Lai, C., Zhao, N., and Li, X. (2009). Molecular self-assembly synthesis of nano-sphere of La-containing hexagonal mesoporous solid. *J. Alloys Compd.* 484, 841–845. doi: 10.1016/j.jallcom.2009.05.054
- Wu, J. J., Zheng, K., Huang, X. T., Liu, J. Y., Liu, H. M., Boccaccini, A. R., et al. (2019). Thermally triggered injectable chitosan/silk fibroin/bioactive glass nanoparticle hydrogels for in-situ bone formation in rat calvarial bone defects. *Acta Biomater.* 91:60. doi: 10.1016/j.actbio.2019.04.023
- Xia, X., Pethe, K., Kim, R., Ballell, L., Barros, D., Cechetto, J. (2014). Encapsulation of anti-tuberculosis drugs within mesoporous silica and intracellular antibacterial activities. *Nanomaterials* 4, 813–826. doi: 10.3390/nano4030813
- Yin, W., Yu, J., Lv, F., Yan, L., Zheng, L., Gu, Z., et al. (2016). Functionalized Nano-MoS₂ with peroxidase catalytic and near-infrared photothermal activities for safe and synergetic wound antibacterial applications. *ACS Nano* 10, 11000–11011. doi: 10.1021/acsnano.6b05810
- Yuan, Q., Zhang, Y., Chen, T., Lu, D., Zhao, Z., Zhang, X., et al. (2012). Photon-manipulated drug release from a mesoporous nanocontainer controlled by azobenzene-modified nucleic acid. *ACS Nano* 6, 6337–6344. doi: 10.1021/nn3018365
- Zhang, S. H., Sun, C. X., Zeng, J. F., Sun, Q., Wang, G. L., Wang, Y., et al. (2016). Ambient aqueous synthesis of ultrasmall PEGylated Cu_{2-x}Se Nanoparticles as a multifunctional theranostic agent for multimodal imaging guided photothermal therapy of cancer. *Adv. Mater.* 28, 8927–8936. doi: 10.1002/adma.201602193
- Zhang, Y. L., Xia, L. G., Zhai, D., Shi, M. C., Luo, Y. X., Feng, C., et al. (2015). Mesoporous bioactive glass nanolayer-functionalized 3D-printed scaffolds for accelerating osteogenesis and angiogenesis. *Nanoscale* 7, 19207–19221. doi: 10.1039/C5NR05421D
- Zhang, Y. Y., Lv, F., Cheng, Y. R., Yuan, Z. P., Yang, F., Liu, C. H., et al. (2019). Pd@Au bimetallic nanoplates decorated mesoporous MnO₂ for synergistic nucleus-targeted NIR-II photothermal and hypoxia-relieved photodynamic therapy. *Adv. Healthc. Mater.* 9:1901528. doi: 10.1002/adhm.201901528
- Zhou, L., Zheng, H., Wang, S., Zhou, F., Lei, B., and Zhang, Q. (2020). Biodegradable conductive multifunctional branched poly(glycerol-amino acid)-based scaffolds for tumor/infection-impaired skin multimodal therapy. *Biomaterials* 262:120300. doi: 10.1016/j.biomaterials.2020.120300

Conflict of Interest: The authors declare that the research was conducted in the absence of any commercial or financial relationships that could be construed as a potential conflict of interest.

Copyright © 2020 Ma, Ma, Chen, Li, Liu, Ma, Mao, Yang, Ma and Wang. This is an open-access article distributed under the terms of the Creative Commons Attribution License (CC BY). The use, distribution or reproduction in other forums is permitted, provided the original author(s) and the copyright owner(s) are credited and that the original publication in this journal is cited, in accordance with accepted academic practice. No use, distribution or reproduction is permitted which does not comply with these terms.